A mouse model of maternal obesity leads to uterine natural killer (uNK) cell activation and uterine artery remodeling defects

Jennet Baltayeva[*,§], Barbara Castellana[*,§], Danielle L. Mara[*], Julian K. Christians[#,*], Alexander G. Beristain[*,§]

[*] British Columbia Children's Hospital Research Institute, Vancouver, Canada.
[§] Department of Obstetrics & Gynecology, The University of British Columbia, Vancouver, Canada.
[#] Department of Biological Sciences, Simon Fraser University, Burnaby, Canada.

Running Title: Effects of obesogenic diet on uterine natural killer (uNK) cell biology

To whom correspondence should be addressed: Alexander G. Beristain, British Columbia Children's Hospital Research Institute, Department of Obstetrics & Gynecology, The University of British Columbia, Vancouver, British Columbia, Canada. V5Z 4H4. Tel: (604) 875-3573; E-mail: aberista@mail.ubc.ca

Keywords: Pregnancy, natural killer cell, uterus, placenta, diet-induced obesity, spiral artery remodeling, high-fat/high-sucrose diet

FUNDING

This work was supported by a BC Children's Hospital Healthy Starts Catalyst Grant (to AGB and JKC) and a Canadian Institutes of Health Research Open Operating Grant (201403MOP-325905-CIA-CAAA) (to AGB).

ABSTRACT

Maternal obesity associates with multiple adverse reproductive outcomes, negatively affecting the health and survival of both the mother and the fetus. The contributory effects of obesity on adipose-derived immune changes have been well established, however the mechanisms that link obesity to pregnancy complications remain unclear. Proper development of the placenta and establishment of utero-placental vasculature is essential in early pregnancy to allow for optimal fetal growth and survival. Uterine immune cells, particularly uterine natural killer (uNK) cells, play fundamental roles in promoting these events. Using an obesogenic high-fat/high-sucrose (HFD) mouse model of maternal obesity, uNK cells and placenta/uterine vascular remodeling were examined at gestational days (Gd) 10.5 and 14.5 of pregnancy. While mice fed a HFD 13 weeks prior to pregnancy significantly gained more weight than control mice fed a low-fat/no-sucrose diet (LFD), fetal survival was not different in either diet. At Gd 10.5, HFD had no effect on total uNK proportions, nor did it affect proportions of distinct CD122+/CD49a tissue resident or CD122+/DX5+ conventional uNKs. However, HFD resulted in increased proportions of NCR1+ uNK and overall heightened uNK activity. Moreover, HFD resulted in impairments in uterine vascular remodeling at Gd10.5. By Gd14.5, uterine artery defects were no longer observed and placental structure was comparable between HFD and LFD mice. Gene analysis of IFNγ, TNFα and VEGFA in Gd10.5 uNK indicated that, while not significant, a HFD leads to subtle alterations in uNK cytokine gene expression. These findings show that HFD in mice results in changes in uNK biology and temporary uterine artery remodeling impairments. Further, this work establishes insight into the cellular changes occurring in early pregnancy as a result of HFD exposure.

INTRODUCTION

Obesity affects more than half a billion adults worldwide and has become a global epidemic[1]. Consistent with trends in general population, rates of obesity among women of childbearing age are increasing rapidly[2–4]. Pre-pregnancy obesity is recognized as a high-risk state because of its association with multiple adverse obstetric and perinatal outcomes including miscarriage, preeclampsia, preterm birth and intrauterine fetal demise[5]. Providing the interface between the mother and developing baby, the placenta plays a key role in mediating the effect of the adverse maternal environment to the fetus[6,7]. Studies in rodents have established the effect of maternal obesity on placental dysfunction reflected in part by vascular impairments within the maternal-fetal interface[8–10]. However, the molecular mechanisms that link detrimental pregnancy outcomes to pre-gravid obesity are poorly understood.

Optimal placental function and overall pregnancy success is largely dependent upon the proper establishment of fetal and maternal circulations within the fetal-maternal interface; these processes are controlled by tightly regulated angiogenic and vascular remodeling programs[11,12]. Early stages of blood vessel growth, branching, pruning, and remodeling are controlled by diverse leukocyte populations that localize within the decidual microenvironment of the uterus[13,14]. Uterine natural killer (uNK) cells constitute the most abundant immune cell population within both human and murine uterus in early pregnancy[15–17], and genetic studies in mice show that these cell types are major contributors to uterine vascular transformations[18–20].

Despite a number of physiological and anatomical differences that exist between human and murine pregnancy, uNK cell function and regulation of uNK-governed events are comparable between these species. uNK cells in human pregnancy facilitate the initial stages of arterial vascular transformation and control extravillous trophoblast invasion[13]. While distinct uNK subtypes in human decidua are less well-defined, at least two functionally distinct populations of uNK cells in mice have

been classified, and are characterized by their reactivity to Dolichos biflorus agglutin (DBA) and cell-surface expression of CD49a and DX5[21]. DBA^+ $CD49a^+DX5^{+/-}$ define a tissue-resident uNK population and predominantly mediate angiogenic growth factor production (VEGFA, PGF)[21,22], whereas DBA^- $CD49a^-DX5^+$ identify a conventional uNK population that preferentially produces IFNγ and play roles in uterine vasculature remodeling[18,21,22]. In summary, uNK cell-directed processes are critical to successful pregnancy.

Obesity is characterized by adipose tissue expansion and infiltration of immune cells, including macrophages, T lymphocytes, B cells, mast cells, and neutrophils[23–25]. Along with increase in numbers of immune cells, obesity/adipose-related environment alters leukocyte activation within adipose tissue, potentiating the secretion of pro-inflammatory cytokines that have both local and distal effects[26]. For example, obesity associates with aberrant activation of liver[27] and pancreatic[28] macrophages, and alterations in the macrophage immune cell function is thought to contribute to obesity-related metabolic diseases[29]. This indicates that obesity-related immune alterations within reproductive tissues like the uterus and placenta may also be impacted. Since uNK cell differentiation, maturation, and activity are highly influenced by soluble factors like cytokine and hormones, as well as through direct cellular interactions[30,31], the uterine microenvironment in obesity may play an important role in shaping uNK-related processes that affect pregnancy.

In this study, we aimed to investigate the impact of high-fat/high-sucrose obesogenic diet (HFD) on uNK cell function and placental development in early-mid pregnancy in mice. We demonstrate that uNK cells from HFD mice show changes in natural killer cell receptor composition and activation status. Importantly, a HFD promoted impaired spiral artery remodeling within an early-mid pregnancy and potentiated the differential expression of uNK-derived cytokines at mid-gestation.

Together, our work provides novel insight into HFD-induced changes in uNK cell function and uterine vascular transformations in early-mid pregnancy.

1 **RESULTS**

2 **Maternal obesity drives inflammation in early pregnancy with no effect on fetal viability**

3 To investigate the effects of maternal obesity on uterine natural killer cell biology and placental
4 development, we established a murine model of diet-induced obesity, where female C57BL/6J mice
5 were fed a high-fat/high-sucrose diet (HFD) or low-fat/no-sucrose diet (LFD) over the period of 13
6 weeks before mating and during pregnancy (Figure 1A). As expected, exposure to HFD resulted in a
7 significant body weight gain over the course of 13 weeks (Figure 1B). Similar to this trend, HFD-fed
8 mice continued gaining weight at a progressive rate throughout gestation (Figure 1C). HFD was also
9 associated with the induction of pro-inflammatory state in early-mid pregnancy (Gd10.5), reflected by
10 the heightened maternal serum concentrations of TNFα, an important mediator of systemic
11 inflammation[32] (Figure 1D). Despite having profound effects on maternal parameters, HFD did not
12 affect overall fetal survival, where numbers of live conceptuses and a rate of fetal resorption remained
13 unchanged between HFD- and LFD-fed mice at Gd14.5 (Figure 1E, F). This finding is consistent with
14 our previous work showing that while maternal HFD leads to changes in maternal physiology and
15 metabolic profile, including a significant weight gain before and during pregnancy, hyperglycemia and
16 glucose intolerance, detrimental consequences on fetal parameters are not observed[33]. In summary, we
17 have developed a mouse model of obesity in pregnancy defined by inflammatory and metabolic
18 disturbances.

19

20 **HFD leads to increase in proportions of NCR1^{+} uNKs at Gd10.5 without disturbing tr-uNK and**
21 **c-uNK ratios**

22 NKs in the murine uterus are made up of DBA^{+}CD49a^{+}DX5$^{+/-}$ tissue-resident uNK (tr-uNK)
23 and DBA^{-}CD49a^{-}DX5^{+} conventional uNK (c-uNK) cell populations[21]. To this end, we first investigated

whether the HFD would alter uNK numbers in early pregnancy by histologically examining the DBA^+ cells at Gd7.5 and Gd10.5. Although DBA^+ cells from both HFD and LFD uterine tissues underwent normal age-related increase in their quantity[34], their numbers were not affected by diet (Figure 2A). Following this, we went on to examining the proportions of total leukocytes ($CD45^+$) and uNKs ($CD3^-$ $CD122^+$), as well as specific tr-uNK and c-uNK sub-populations at Gd10.5 by flow cytometry (Figure 2B). We chose Gd10.5 to be an appropriate time point for uNK-related assessments, since these uNK cells peak in numbers at mid-gestation[21]. HFD had a little effect on total immune cell and uNK cell proportions (Figure 2C). Confirming our qualitative observations, HFD did not exert any measurable effect on the tr-uNK and c-uNK in-utero balance (Figure 2D).

Natural cytotoxicity receptor 1 (NCR1) is a known activating receptor expressed on uNKs that is essential for uNK cell maturation and function, including blood vessel remodeling[35,36]. Thus, to further elucidate effects of maternal HFD on uNK cell biology, we assessed uNK NCR1 expression. Interestingly, we found that HFD drives an increase in the proportion of $CD122^+NCR1^+$ uNK; NCR1 expression levels [measured by median fluorescent intensity (MFI)] are not affected (Figure 2E). These findings suggest that maternal obesity manifests in subtle changes in uNK cell composition in early-mid pregnancy, promoting acquisition of NCR1.

HFD promotes a shift in uNKs towards an activated phenotype at Gd10.5

Previous studies report that NCR1 is important for uNK cell maturation, measured by the increase in uNK cell dimeter/size[36]. Since we observed HFD-induced changes in proportions of $NCR1^+$ uNK cells at Gd10.5, we assessed whether the maturation and activation is affected following HFD exposure. As NCR1 is expressed predominantly by DBA^+ cells at Gd10.5[36], we focused on measuring DBA^+ cell diameters in histological sections of utero-placental tissues from HFD- and LFD-fed mice

by DBA-labeling fluorescence microscopy. Differences in DBA^+ uNK cell diameters between diet groups were not observed (Figure 3A). Following this, we proceeded to investigate the expression of CD69, an early NK cell activation marker[37] in $CD122^+$ and $CD122^+NCR1^+$ uNK cells by flow cytometry (Figure 2B). Notably, expression levels (MFI) of CD69, but not $CD69^+$ cell proportions, were significantly elevated in $CD122^+$ and $CD122^+NCR1^+$ uNK cell populations as a result of HFD (Figure 3C, D). These observations suggest that while not directly affecting maturation of uNK cells, HFD promotes a shift towards the activation of these cells in early-mid pregnancy.

HFD impairs spiral artery remodeling in mid pregnancy

Early pregnancy spiral artery (SA) remodeling is a process controlled and regulated by uNKs[38]. NCR1 is known to play a role in uNK-mediated spiral artery remodeling[36]. Thus, we next set out to address whether HFD-induced changes observed in uNK cell activation and NCR1 expression may translate into alterations in artery remodeling. Measurements of arterial wall and lumen areas (μm^2) and their ratios were performed for all the spiral arteries present in the deciduas of HFD- and LFD-fed mice at Gd10.5 (Figure 4A). We also qualitatively assessed decidual artery smooth muscle actin (SMA) expression and localization via immunofluorescence microscopy at two gestational time-points: Gd7.5 (prior to initiation of vascular remodeling) and Gd10.5 (when remodeling is at its peak)[39]. Vascular remodeling is accompanied by the loss of SMA surrounding the vessel walls, and as such, SMA layer integrity can be used as a surrogate measure of remodeling[40]. At Gd7.5 the SMA layer was intact surrounding vessels in placentae of mice from both HFD- and LFD-fed (Figure 4B). However, by Gd10.5, partial loss of SMA integrity was observed in HFD mice, while LFD mice exhibited robust loss of SMA staining (Figure 4B). Further, at Gd10.5, HFD-fed mice had smaller vessel sizes and thicker arterial walls (Figure 4A), and accordingly had significantly higher wall:lumen ratios at Gd10.5

(Figure 4C). Notably, the impairments in blood vessel remodeling observed at Gd10.5 in HFD mice were no longer observed by Gd14.5 (Figure 4D). Specifically, uterine arteries from both LFD and HFD-fed mice presented with dilated lumens and thin walls, indicative of proper remodeling (Figure 4D). This suggests that maternal HFD disrupts uNK-mediated vascular remodeling in early-mid gestation, but that compensatory processes enable proper artery remodeling by mid-gestation.

Placental morphology at Gd14.5 is unaffected by HFD-induced obesity

Through regulation of angiogenesis, vascular remodeling and trophoblast invasion, uNKs play a prominent role in placental development[21]. HFD-induced alterations in uNK cell composition and activation, as well as impaired SA remodeling in mid-pregnancy suggest that changes in placental development may also be present. To assess this, we have measured the areas (mm^2) of placental layers from HFD- and LFD-fed mice at Gd14.5, a time-point where the murine placenta is properly developed and subdivided into three definitive layers: labyrinth (L), junctional zone (Jz) and decidua (D)[41]. Assessment of total placental area did not reveal any significant differences between diet groups (Figure 5A). Moreover, the areas of individual placental layers were not altered in the context of maternal HFD (Figure 5 B, C, D). Together our findings imply that HFD-related disturbances in early-mid gestation do not persist at late gestation, which could provide an explanation as to why the fetal parameters were undisturbed following maternal exposure to HFD.

HFD potentiates altered expression of uNK-derived cytokines

Since HFD increased proportions of $NCR1^+$ uNKs and induced uNK cell activity, we next set out to examine if these uNK-related changes translate into altered uNK-directed cytokine expression.

Using real-time qPCR approach, we measured relative expression levels of 4 uNK-derived genes known to regulate angiogenesis (VEGFA) and remodeling in uterine arteries (IFNγ, TNFα, MMP-2)[18,39,42,43] from flow cytometry sorted Gd10.5 total uNKs. Large variances in expression of these factors were observed in uNK exposed to either diet, with expression of MMP-2 being particularly heterogeneous (Figure 6B). Although not significant, HFD induced a modest trend in increased IFNγ and TNFα, and decreased VEGFA expression (Figure 6A, C, D) (p=0.13 for IFNγ; p=0.11 for TNFα; p=0.11 for VEGFA). Our data suggest that these potential alterations in uNK cytokine expression may be due to the HFD-related changes in uNK cell composition and activation.

DISCUSSION

In this study, we examine the effects of maternal HFD on uNK cell biology and uterine vascular transformations in early-mid pregnancy. We demonstrate that maternal HFD does not alter total uNK numbers or subsets of tissue-resident or conventional cells. However, a HFD results in a selective increase in the proportion of NCR1+ uNK and globally promotes uNK activation. Heightened uNK activity translated into trends towards increased IFNγ and TNFα expression and decreased VEGFA expression. Importantly, we show that a HFD leads to impaired spiral artery remodeling at mid-gestation, although this is no longer observed by late gestation. Notably, early pregnancy artery defects do not impact placental morphology or fetal viability. Together, our findings show how an obesogenic diet instructs changes in uNK cell function and uterine vasculature and provide novel insight into underlying cellular changes that may contribute to obesity-related pregnancy disorders.

To our knowledge, this is the first study to examine the effects of HFD on uNK cell proportions and states of activation in pregnancy. In contrast to a previous report that examined the impact of a maternal western diet on mouse NK cells within draining inguinal lymph nodes of the uterus[9], our study directly examines uNK cells within the maternal-fetal interface. Since uNK within mucosal tissues of the uterus are distinct from peripheral and lymphatic NKs[44–46], the findings from our work accurately describe how maternal obesity impacts immune cell function at the maternal-fetal interface. Notably, we show that a HFD does not affect total leukocyte or uNK cell proportions. Due to the emerging evidence supporting the presence of two distinct uNK subpopulations that differ in function[21,22] in the murine uterus, we thought it is important to decipher the effects of HFD on the balance of these cells *in-utero*. Consistent with our findings that total uNK proportions are unchanged in response to a HFD, neither tr-uNK nor c-uNK proportions were affected. This implies that a HFD may not alter uNK cell infiltration or expansion into/within the uterus in early pregnancy, a finding that

is in contrast with other studies examining the effect of a HFD on NK infiltration into organ/tissue sites like fat tissue[47,48].

Our focus on NCR1 stems from previous work reporting that *Ncr1*$^{-/-}$ mice exhibit defects in decidual angiogenesis and uterine vascular remodeling[36]. Notably, inhibition of NCR1 delays uNK cell maturation and activation, reflected by smaller cell diameters and reductions in cytokine production[49]. Here, we demonstrate that in mid-pregnancy a HFD leads to an increase in NCR1^{+} uNK cell proportions. NCR1 is predominantly expressed by DBA^{+} tr-uNKs[36], and since we did not observe changes in tr-uNK or c-uNK proportions, the increase in NCR1^{-}expressing uNKs may indicate that DBA^{-} c-uNK cells exposed to a HFD are instructed to acquire or increase expression of NCR1. This finding suggests that uNK exposed to a HFD undergo a state of NCR1-related compensation to enhance or rescue impaired artery remodeling. Alternatively, the increase in proportions of NCR1^{+} uNK may also translate to enhanced uNK cytotoxicity. Further work is required to more accurately dissect the significance of NCR1-related changes resulting from HFD.

One of the additional measures of uNK activation is expression of the early activation marker CD69[17]. We show that both tr- and c- uNK cells express higher levels (MFI) of CD69 in HFD-fed mice. As expected, activation of uNKs was reflected by changes in their cytokine expression (increase in IFNγ and TNFα, decrease in VEGFA). Although not statistically significant, likely due to an under-powered sample size, we believe that this finding provides important insight into uNK functional changes in HFD. uNK-derived IFNγ is critical for triggering pregnancy-induced uterine vascular modification, required for optimal placentation[18]. We believe that activation of uNK cells and a potential increase in their IFNγ expression at Gd10.5 in HFD-fed mice is a compensatory mechanism employed by these cells to assist in catching up with the vascular remodeling. This might explain why HFD-induced impairment of spiral artery remodeling in our model is observed at Gd10.5 but not

Gd14.5. Since vascular remodeling is important for proper placentation, it was not surprising that placental morphology and areas of individual placental layers in HFD-fed were not affected at Gd14.5.

The changes associated with uNK activation and cytokine expression in mid-pregnancy affected by HFD need to be interpreted with care. While, it may be a compensatory mechanism employed by these cells to rescue the defective vascular remodeling, it also may be the case that the artery remodeling is impaired as a result of delayed activation and maturation of uNKs. Thus, it will be important to examine the activation/maturation phenotype of uNKs throughout the gestation, starting from Gd6.5 when these cells appear in the murine decidua[17], in the context of an obesogenic environment to decipher the dynamics of HFD-induced effects on uNKs.

Our previous study investigating the effects of maternal obesity on uNK cell function in human pregnancy shows that obesity leads to fewer uNK cells within decidual tissues and, similar to our findings in mice exposed to a HFD, associates with impaired vascular remodeling in early gestation[50]. These similarities between obesity- and obesogenic diet-driven structural changes within uterine tissue of human and mouse suggest that obesity/HFD in either species results in uNK cell alterations that predispose to impairments in uterine health and function.

We report that fetal viability in late pregnancy (Gd14.5) is not affected by HFD. This is consistent with our findings from a previous study employing the same diet conditions and strain of mice, where pregnancy outcomes (fetal survival, fetal and placental weights) were not affected by a HFD[33]. However, the impact of obesogenic-diets on fetal health and pregnancy outcome in rodents is not consistent, where in contrast to our findings indicating that a HFD does not affect fetal survival or placental structure, other studies have shown that HFD exposure in pregnancy results in both reduced[51,52] and increased[53,54] fetal weight, and reduced placental labyrinth[55] and junctional zone[51] thickness, or no differences in placental weights[52,56,57]. The variation in pregnancy outcomes between

studies may be due to differences in animal strains, maternal age, maternal weight gain, composition of the diet in terms of micro- and macronutrient content and the duration of time animals are exposed to the diet.

uNKs are specialized immune cells that play an important role in coordinating reproductive success. Deviations in normal uNK function may contribute to defective vascular modifications at the maternal-fetal interface implicated in pregnancy complications. Our study provides insight into a potential mechanism of maternal HFD-driven uNK activation and defective spiral artery remodeling in mid-pregnancy using a mouse model, thus identifying possible cellular contributors to obesity-related poor pregnancy outcomes. Maternal obesity continues posing serious consequences on reproductive health, thus further dissecting obesity-driven immune and cellular alterations within the uterus will be of substantial importance.

METHODS

Animals. Mouse experiments were carried out in accordance with the guidelines of the Canadian Council on Animal Care and approved by SFU University Animal Care Committee (protocol 1094) and the UBC Animal Care Committee (protocol A17-0060). C57BL/6J mice were purchased from the Jackson Laboratory (Bar Harbor, ME, USA). Animals were housed under standard conditions in groups of max. 5 mice in individually ventilated cages with water and food available *ad libitum*, under a 12:12h light/dark cycle.

High-fat/high sugar obesogenic model. At 9 weeks of age, females were placed on either a high-fat, high-sucrose diet (HFHS; 45% kcal fat, 35% carbohydrate (including 17% kcal sucrose), 20% kcal protein, 4.73 kcal/g, D12451, Research Diets, New Brunswick, NJ) or a nutrient-matched low-fat, no-sucrose control diet (CON; 10% kcal fat, 70% kcal carbohydrate (corn starch and maltodextrin), 20% kcal protein, 3.85 kcal/g, D12450K, Research Diets). Females were kept on the experimental diets for 13 weeks prior to being paired with male studs. The appearance of a plug the next morning was taken as day 0.5 of pregnancy. Because not all females became pregnant when first paired, some had been on the experimental diet for 13–19 weeks at the start of pregnancy. On days 7.5, 10.5 and 14.5 of pregnancy females were euthanized and their blood collected via cardiac puncture. The utero-placental tissues with multiple implantation sites were collected from each mouse.

ELISA measurements of serum TNFα. Serum was purified from whole blood of females sacrificed at Gd10.5 of pregnancy using serum separator tubes following standard procedures. Serum levels of TNFα were determined using commercially available Mouse TNFα ELISA kit (R&D systems) according to manufacturer's protocol.

1

2 **Decidual leukocyte preparations.** For examination of uNK cell populations, murine
3 implantation sites were separated from uterine tissues and were mechanically and enzymatically
4 processed to obtain single-cell suspensions. In brief, tissues were washed extensively in cold
5 phosphate-buffered saline (PBS; pH 7.4), and following this, tissues were minced with a razor blade
6 and subjected to a 30-minute enzymatic digestion at 37 °C in 3 mL of 1:1 DMEM/F12 media (Gibco,
7 Grand Island, NY; 200 mM L-glutamine) with 1X-collagenase/hyaluronidase (10X stock; StemCell
8 Technologies, Vancouver, Canada), 80 μg/mL DNaseI (Sigma, St. Louis, MO),
9 penicillin/streptomycin, and Anti antimycotic solution (100X dilution, Gibco). Single cell suspensions
10 were passed through a 100μm strainer and decidual leukocyte enrichment was performed by Percoll
11 (GE Healthcare) density gradient (layered 40%/80%) centrifugation. To avoid red blood cell
12 contamination, cell mixture was briefly incubated with NH_4Cl. Decidual leukocytes were immediately
13 used for uNK isolation by fluorescence activated cell sorting (FACS) or cell-surface marker
14 characterization via flow cytometry analyses.

15

16 **Flow cytometry.** Flow cytometry analyses were carried out following a standard protocol. In
17 brief, 0.5x10^6 isolated leukocytes were incubated with Fc Block (anti-CD16/CD32 antibody at 1:35
18 dilution in PBS; BD Pharmingen) for 10 min on ice to prevent non-specific binding. Cell suspensions
19 were further incubated with fluorescent-conjugated antibodies directed against cell-surface markers for
20 30 minutes at 4°C. The following antibodies were used: APC ef780 CD3e (1:50; clone 145-2C11;
21 eBioscience), ef450 CD45 (1:100; clone 30-F11; eBioscience), PerCP710 CD122 (1:100; clone TM-
22 b1; eBioscience), APC CD122 (1:35; clone TM-Beta 1; BD Pharmingen), APC CD49a (1:50; clone
23 HMα1; BioLegend), PeCy7 CD49b (1:100; clone DX5; eBioscience), APC CD69 (1:25; clone H1.2F3;

eBioscience), PeCy7 NKp46 (1:50; clone 29A1.4; eBioscience). Following staining, cells were re-suspended in 7-AAD viability staining solution (at 1:25 dilution in PBS+ 2%FBS +1% penicillin/streptomycin; eBioscience). Samples were acquired on an LSRII FACS (BD Biosciences) and data was analysed by FlowJo 5.0 software (Tree Star, Inc., Ashland, OR, USA).

Immunohistochemistry, IF microscopy and morphometry. Implantation sites from Gd7.5, Gd10.5 and Gd14.5were fixed in 4% paraformaldehyde for 24-48h followed by processing into paraffin blocks. Six-µm sections were stained with hematoxylin and eosin (H&E) according to standard methods. For IF staining, tissues underwent antigen retrieval by heating slides in a microwave for 5 minutes in 30-second intervals in a sodium citrate buffer (pH 6.0). Sections were then incubated in a blocking solution (5% bovine serum albumin (BSA) in Tris-buffered saline with 0.05% Tween-20 (TBST)) for 1 hour at room temperature. Further, samples were incubated with the following antibodies overnight at 4°C: rabbit polyclonal alpha-smooth muscle actin (1:200; Abcam) and biotinylated DBA (1:100; Vector Laboratories). Slides were incubated with Alexa Fluor 568/488–conjugated streptavidin and goat anti-rabbit secondary antibodies (Life Technologies) for 1 hour at room temperature. Glass coverslips were mounted onto slides using ProLong Gold anti-fade reagent containing DAPI (Life Technologies).

DBA^+ cell assessments. DBA^+ cell quantities in Gd7.5 and Gd10.5 implantation sites were calculated based on DBA fluorescence intensity threshold. Slides were imaged using a 20x Plan-Apochromat/0.80 NA or a 40x EC-Plan-Neofluar/0.9 PoI objective (Carl Zeiss). Data was processed and analyzed using ZenPro software (Carl Zeiss). DBA^+ cell diameters in Gd10.5 implantation sites were measured by randomly selecting 100 DBA^+ uNK cells from each implantation site. Slides were imaged using a 40x EC-Plan-Neofluar/0.9 PoI objective (Carl Zeiss). Using ImageJ v1.50 software

(NIH), the diameters of these cells were measured across their longest and shortest axes; an average of both values was used for statistical analysis. All images were obtained using Axiocam 506 monochrome digital camera (Carl Zeiss).

Spiral artery remodeling assessments. Spiral artery remodeling measurements were performed on H&E stained slides. For Gd10.5, (HFD: n=9 implantation sites from 8 independent pregnancies; LFD: n=11 implantation sites from 9 independent pregnancies) all of the spiral arteries within the decidua were measured in triplicate (three sections 48μm apart from each other). For Gd14.5, (HFD: n=18 implantation sites from 7 independent pregnancies; LFD: n=17 implantation sites from 6 independent pregnancies) all of the spiral arteries within the decidua were measured in duplicate (two sections 48μm apart from each other). Size of arterial walls and lumens was determined by measuring cross-sectional areas with ImageJ v1.50 software (NIH). Wall:lumen ratios were calculated by dividing the arterial wall area (μm^2) into the artery lumen area (μm^2). Slides were imaged using a 20x Plan-Apochromat/0.80 NA objective (Carl Zeiss). All images were obtained using Axiocam 105 color digital camera (Carl Zeiss).

Placental morphology assessments. H&E stained slides of Gd14.5 implantation sites were used for placental morphology measurements. Total area (μm^2) and areas of each individual placental layer (μm^2) were measured using ImageJ v1.50 software (NIH). To normalize for differences in total placental area among the measurements, individual layer area was expressed as a percentage of total area at each measurement point. Slides were imaged using 10x N-Achroplan/0.25 Ph1 objective (Carl Zeiss). All images were obtained using Axiocam 105 color digital camera (Carl Zeiss).

RNA preparation, cDNA synthesis, and qPCR. Prior to RNA extraction, CD45+CD3-CD122+ uNK cells from Gd10.5 implantation sites were isolated by FACS using a FACSAria flow cytometry (BD Biosciences). Total RNA was prepared from isolated uNKs using TRIzol LS reagent (Ambion) following by RNeasy MinElute Cleanup (Qiagen) and DNase treatment (Ambion) according to manufacturers' protocols. RNA purity was confirmed using a NanoDrop Spectrophotometer (Thermo Fisher Scientific) and Agilent 2100 Bioanalyzer (Agilent). Only RNA samples having an RNA integrity number (RIN) greater than 8.0 were used. RNA was reverse-transcribed using a first-strand cDNA synthesis kit (Quanta Biosciences) and subjected to qPCR (ΔΔCT) analysis, using PerfeCTa SYBR Green FastMix Low ROX (Quanta Biosciences) on an ABI ViiA 7 Real-Time PCR system (Thermo Fisher Scientific). Forward and reverse primer sets used as previously described: *VEGFA* (F: 5'-GTGCACTGGACCCTGGCTTTA-3', R: 5'-GGTCTCAATCGGACGGCAGTA-3')[58]; *IFNγ* (F: 5'- TCAGCAACAGCAAGGCGAAAAAG-3', R: 5'-ACCCCGAATCAGCAGCGACTC-3')[59]; *MMP2* (F: 5'-GCTGTATTCCCGACCGTTGA-3', R: 5'-TGGTCCGCGTAAAGTATGGG-3')[60]; *TNFα* (F: 5'-CATCTTCTCAAAATTCGAGTGACAA-3', R: 5'-TGGGAGTAGACAAGGTACAACCC-3')[61]; *HPRT* (F: 5'-CTGGTGAAAAGGACCTCTCG-3', R: 5'-TGAAGTACTCATTATAGTCAAGGGCA-3')[62]. All raw data were analyzed using QuantStudio V1.3 software (Thermo Fisher Scientific). The threshold cycle (CT) values were used to calculate relative gene expression levels. Values were normalized to *HPRT* transcripts.

Statistical analysis. Statistical significance for all data was assessed by unpaired two-tailed Student's t-tests. $P < 0.05$ was considered significant. Statistical analyses were performed using Prism7 software (GraphPad Software, Inc.)

ACKNOWLEDGEMENTS

We are grateful to staff from Simon Fraser University Animal Care facility for their assistance. We would like to extend our gratitude to BCCHRI Flow Core Facility Manager, Dr. Lisa Xu, for her expertise and assistance in cell sorting of uNK cells.

CONFLICT OF INTEREST

The authors declare no conflict of interest.

AUTHOR CONTRIBUTIONS

AGB and JKC designed the research. JB, BC, DM, JKC and AGB performed the experiments. JB, AGB and JKC analysed the data and wrote the paper. All authors read and approved the manuscript.

REFERENCES

1. World Health Organisation. WHO | Obesity and overweight. *WHO* (2017).
2. Statistics Canada. Canadian Community Health Survey: Obesity among children and adults. Available at: http://www.statcan.gc.ca/daily-quotidien/050706/dq050706a-eng.htm. (Accessed: 26th February 2018)
3. Ogden, C. L., Carroll, M. D., Kit, B. K. & Flegal, M. Prevalence of Childhood and Adult Obesity in the United States, 2011–2012. *Jama* **311,** 806–814 (2016).
4. Public Health Agency of Canada. Obesity in Canada: A joint report from the Public Health Agency of Canada and the Canadian Institute for Health Information. *Report No. Cat.: HP5-107/2011E-PDF.* (2011). Available at: https://www.canada.ca/en/public-health/services/health-promotion/healthy-living/obesity-canada.html. (Accessed: 26th February 2018)
5. Leddy, M. A., Power, M. L. & Schulkin, J. The impact of maternal obesity on maternal and fetal health. *Rev. Obstet. Gynecol.* **1,** 170–8 (2008).
6. Denison, F. C., Roberts, K. A., Barr, S. M. & Norman, J. E. Obesity, pregnancy, inflammation, and vascular function. *Reproduction* **140,** 373–385 (2010).
7. Schmatz, M., Madan, J., Marino, T. & Davis, J. Maternal obesity: The interplay between inflammation, mother and fetus. *Journal of Perinatology* **30,** 441–446 (2010).
8. Hayes, E. K. *et al.* Trophoblast invasion and blood vessel remodeling are altered in a rat model of lifelong maternal obesity. *Reprod. Sci.* **21,** 648–57 (2014).
9. Parker, V. J., Solano, M. E., Arck, P. C. & Douglas, A. J. Diet-induced obesity may affect the uterine immune environment in early–mid pregnancy, reducing NK-cell activity and potentially compromising uterine vascularization. *Int. J. Obes.* **38,** 766–774 (2014).

1 10. Hayes, E. K. *et al.* Adverse fetal and neonatal outcomes associated with a life-long high fat
2 diet: Role of altered development of the placental vasculature. *PLoS One* **7,** (2012).
3 11. Osol, G. & Moore, L. G. Maternal Uterine Vascular Remodeling During Pregnancy.
4 *Microcirculation* **21,** 38–47 (2014).
5 12. Bardin, N., Murthi, P. & Alfaidy, N. Normal and Pathological Placental Angiogenesis. *BioMed*
6 *Research International* **2015,** (2015).
7 13. Cartwright, J. E., Fraser, R., Leslie, K., Wallace, A. E. & James, J. L. Remodelling at the
8 maternal-fetal interface: Relevance to human pregnancy disorders. *Reproduction* **140,**
9 803–813 (2010).
10 14. Faas, M. M. & de Vos, P. Uterine NK cells and macrophages in pregnancy. *Placenta* **56,** 44–
11 52 (2017).
12 15. Moffett-King, A. Natural killer cells and pregnancy. *Nat. Rev. Immunol.* **2,** 656–663 (2002).
13 16. Felker, A. M. & Croy, B. A. Uterine natural killer cell partnerships in early mouse decidua
14 basalis. *J. Leukoc. Biol.* **100,** 645–655 (2016).
15 17. Croy, B. A. *et al.* Imaging of vascular development in early mouse decidua and its
16 association with leukocytes and trophoblasts. *Biol. Reprod.* **87,** 125 (2012).
17 18. Ashkar, A. A., Di Santo, J. P. & Croy, B. A. Interferon gamma contributes to initiation of
18 uterine vascular modification, decidual integrity, and uterine natural killer cell maturation
19 during normal murine pregnancy. *J. Exp. Med.* **192,** 259–70 (2000).
20 19. Barber, E. M. & Pollard, J. W. The uterine NK cell population requires IL-15 but these cells
21 are not required for pregnancy nor the resolution of a Listeria monocytogenes infection. *J.*
22 *Immunol.* **171,** 37–46 (2003).
23 20. Guimond, M.-J. *et al.* Absence of Natural Killer Cells during Murine Pregnancy Is Associated

1 with Reproductive Compromise in TgE26 Mice. *Biol. Reprod.* **56,** 169–179 (1997).

2 21. Gaynor, L. M. & Colucci, F. Uterine natural killer cells: Functional distinctions and influence
3 on pregnancy in humans and mice. *Frontiers in Immunology* **8,** (2017).

4 22. Chen, Z. *et al.* DBA-Lectin Reactivity Defines Mouse Uterine Natural Killer Cell Subsets with
5 Biased Gene Expression1. *Biol. Reprod.* **87,** (2012).

6 23. Xu, H. Obesity and metabolic inflammation. *Drug Discovery Today: Disease Mechanisms* **10,**
7 (2013).

8 24. Stolarczyk, E. Adipose tissue inflammation in obesity: a metabolic or immune response?
9 *Current Opinion in Pharmacology* **37,** 35–40 (2017).

10 25. Patel, P. S., Buras, E. D. & Balasubramanyam, A. The role of the immune system in obesity
11 and insulin resistance. *Journal of Obesity* **2013,** (2013).

12 26. Seijkens, T., Kusters, P., Chatzigeorgiou, A., Chavakis, T. & Lutgens, E. Immune cell crosstalk
13 in obesity: A key role for costimulation? *Diabetes* **63,** 3982–3991 (2014).

14 27. Cai, D. *et al.* Local and systemic insulin resistance resulting from hepatic activation of IKK-β
15 and NF-κB. *Nat. Med.* **11,** 183–190 (2005).

16 28. Ehses, J. A. *et al.* Increased number of islet-associated macrophages in type 2 diabetes.
17 *Diabetes* **56,** 2356–2370 (2007).

18 29. Chawla, A., Nguyen, K. D. & Goh, Y. P. S. Macrophage-mediated inflammation in metabolic
19 disease. *Nat. Rev. Immunol.* **11,** 738–49 (2011).

20 30. Croy, B. A. *et al.* Uterine natural killer cells: Insights into their cellular and molecular
21 biology from mouse modelling. *Reproduction* **126,** 149–160 (2003).

22 31. Cooper, M. A., Fehniger, T. A. & Caligiuri, M. A. The biology of human natural killer-cell
23 subsets. *Trends in Immunology* **22,** 633–640 (2001).

1 32. Bradley, J. R. TNF-mediated inflammatory disease. *Journal of Pathology* **214,** 149–160
2 (2008).
3 33. Chin, E. H. *et al.* A maternal high-fat, high-sucrose diet has sex-specific effects on fetal
4 glucocorticoids with little consequence for offspring metabolism and voluntary locomotor
5 activity in mice. *PLoS One* **12,** (2017).
6 34. Croy, B. A., Yamada, A. T., DeMayo, F. J. & Adamson, S. L. *The Guide to investigation of mouse*
7 *pregnancy*. *The Guide to Investigation of Mouse Pregnancy* **1,** (2015).
8 35. Felker AM, C. B. Natural cytotoxicity receptor 1 in mouse uNK cell maturation and function.
9 *Mucosal Immunol.* (2017). doi:10.1038/mi.2016.126
10 36. Felker, A. M., Chen, Z., Foster, W. G. & Croy, B. A. Receptors for non-MHC ligands contribute
11 to uterine natural killer cell activation during pregnancy in mice. *Placenta* **34,** 757–764
12 (2013).
13 37. Mosimann, B. *et al.* Natural killer cells and their activation status in normal pregnancy. *Int.*
14 *J. Reprod. Med.* **2013,** 906813 (2013).
15 38. Moffett, A. & Colucci, F. Uterine NK cells: Active regulators at the maternal-fetal interface.
16 *Journal of Clinical Investigation* **124,** (2014).
17 39. Lima, P. D. A., Zhang, J., Dunk, C., Lye, S. J. & Anne Croy, B. Leukocyte driven-decidual
18 angiogenesis in early pregnancy. *Cellular and Molecular Immunology* **11,** 522–537 (2014).
19 40. Kieckbusch, J., Gaynor, L. M. & Colucci, F. Assessment of Maternal Vascular Remodeling
20 During Pregnancy in the Mouse Uterus. *J. Vis. Exp.* (2015). doi:10.3791/53534
21 41. Coan, P. M., Ferguson-Smith, A. C. & Burton, G. J. Developmental Dynamics of the Definitive
22 Mouse Placenta Assessed by Stereology1. *Biol. Reprod.* **70,** 1806–1813 (2004).
23 42. Naruse, K. *et al.* Localization of matrix metalloproteinase (MMP)-2, MMP-9 and tissue

1 inhibitors for MMPs (TIMPs) in uterine natural killer cells in early human pregnancy. *Hum.*
2 *Reprod.* **24,** 553–561 (2009).
3 43. Small, H. Y. *et al.* Role of Tumor Necrosis Factor-α and Natural Killer Cells in Uterine Artery
4 Function and Pregnancy Outcome in the Stroke-Prone Spontaneously Hypertensive Rat.
5 *Hypertens. (Dallas, Tex. 1979)* **68,** 1298–1307 (2016).
6 44. Yadi, H. *et al.* Unique Receptor Repertoire in Mouse Uterine NK cells. *J. Immunol.* **181,**
7 6140–6147 (2008).
8 45. Koopman, L. A. *et al.* Human Decidual Natural Killer Cells Are a Unique NK Cell Subset with
9 Immunomodulatory Potential. *J. Exp. Med.* **198,** 1201–1212 (2003).
10 46. Erick, T. K. & Brossay, L. Phenotype and functions of conventional and non-conventional
11 NK cells. *Current Opinion in Immunology* **38,** 67–74 (2016).
12 47. Wensveen, F. M. *et al.* NK cells link obesity-induced adipose stress to inflammation and
13 insulin resistance. *Nat. Immunol.* **16,** 376–385 (2015).
14 48. Duffaut, C., Galitzky, J., Lafontan, M. & Bouloumié, A. Unexpected trafficking of immune cells
15 within the adipose tissue during the onset of obesity. *Biochem. Biophys. Res. Commun.* **384,**
16 482–485 (2009).
17 49. Felker, A. M. & Croy, B. A. Natural cytotoxicity receptor 1 in mouse uNK cell maturation and
18 function. *Mucosal Immunol.* **10,** 1122–1132 (2017).
19 50. Perdu, S. *et al.* Maternal obesity drives functional alterations in uterine NK cells. *JCI Insight*
20 **1,** (2016).
21 51. Mark, P. J. *et al.* A maternal high-fat diet in rat pregnancy reduces growth of the fetus and
22 the placental junctional zone, but not placental labyrinth zone growth. in *Journal of*
23 *Developmental Origins of Health and Disease* **2,** 63–70 (2011).

1 52. King, V., Hibbert, N., Seckl, J. R., Norman, J. E. & Drake, A. J. The effects of an obesogenic diet
2 during pregnancy on fetal growth and placental gene expression are gestation dependent.
3 *Placenta* **34,** 1087–1090 (2013).
4 53. Jones, H. N. *et al.* High-fat diet before and during pregnancy causes marked up-regulation of
5 placental nutrient transport and fetal overgrowth in C57/BL6 mice. *FASEB J.* **23,** 271–278
6 (2009).
7 54. Rosario, F. J., Kanai, Y., Powell, T. L. & Jansson, T. Increased placental nutrient transport in a
8 novel mouse model of maternal obesity with fetal overgrowth. *Obesity* **23,** 1663–1670
9 (2015).
10 55. Song, L. *et al.* Prenatal high-fat diet alters placental morphology, nutrient transporter
11 expression, and mtorc1 signaling in rat. *Obesity* **25,** 909–919 (2017).
12 56. Crew, R. C., Waddell, B. J. & Mark, P. J. Maternal obesity induced by a 'cafeteria' diet in the
13 rat does not increase inflammation in maternal, placental or fetal tissues in late gestation.
14 *Placenta* **39,** 33–40 (2016).
15 57. Kamimae-Lanning, A. N. *et al.* Maternal high-fat diet and obesity compromise fetal
16 hematopoiesis. *Mol. Metab.* **4,** 25–38 (2015).
17 58. Futatsugi, K. *et al.* Obesity-induced kidney injury is attenuated by amelioration of aberrant
18 PHD2 activation in proximal tubules. *Sci. Rep.* **6,** (2016).
19 59. Kang, W., Rathinavelu, S., Samuelson, L. C. & Merchant, J. L. Interferon gamma induction of
20 gastric mucous neck cell hypertrophy. *Lab. Investig.* **85,** 702–715 (2005).
21 60. Dong, H. J. *et al.* The Wnt/β-catenin signaling/Id2 cascade mediates the effects of hypoxia
22 on the hierarchy of colorectal-cancer stem cells. *Sci. Rep.* **6,** (2016).
23 61. Wang, S. *et al.* Tumor suppressor p53 protects mice against Listeria monocytogenes

infection. *Sci. Rep.* **6,** (2016).

62. Demarta-Gatsi, C. *et al.* Immunological memory to blood-stage malaria infection is controlled by the histamine releasing factor (HRF) of the parasite. *Sci. Rep.* **7,** (2017).

1 **FIGURE LEGENDS**

2 **FIGURE 1. Establishment of an obesogenic pregnancy mouse model. A)** Schematic diagram
3 depicting the experimental workflow with low-fat / no-sucrose (LFD) or high-fat / high-sucrose (HFD)
4 diet regime, breeding strategy, pregnancy detection at gestational day (Gd) 0.5, and gestational
5 endpoints (Gd 7.5/10.5/14.5). Shown are uterine horns with multiple conception sites comprised of
6 utero-placental tissues that were allocated for downstream cellular and tissue processing. **B)** Body
7 weight gain prior to pregnancy and **C)** during pregnancy of mice fed either HF diet (HFD; black bars;
8 n=20) or a matched LF diet (LFD; grey bars; n=20). Data represented as mean ± SEM. *p<0.05;
9 **p<0.005. **D)** Number of live conceptuses per mouse observed at Gd14.5. Data represented as mean ±
10 SD. **E)** Percentage of fetal resorption sites per mouse observed at Gd14.5. Data represented as mean ±
11 SD. **F)** Maternal serum levels of TNFα at Gd10.5 (HFD: n=16; LFD: n=13). Data represented as mean
12 ± SD. *P*-values from unpaired Student's t-tests for panels D-F.

13

14 **FIGURE 2. HFD does not affect total uNK proportions, but alters NCR1+ subsets. A)** Number of
15 Dolichos biflorus agglutin positive (DBA+) uterine NK cells (HFD: n=13 implantation sites, LFD: n=9
16 implantation sites) and representative images of DBA immunofluorescence staining within murine
17 implantation sites at Gd7.5 and Gd10.5. Scale bar = 200µm. **B)** Flow cytometry gating strategy to
18 identify and quantify populations of total uterine NK cells: CD3-/CD45+/CD122+; and tissue-resident
19 (tr) and conventional (c) uNKs: CD49a+ or DX5+, respectively. **C)** Scatter plots of total leukocyte and
20 uterine NK cell proportions in HFD (n=19) and LFD (n=14) mice. **D)** Scatter plots of tr- and c- uterine
21 NK cell proportions in HFD (n=18) and LFD (n=14) mice. **E)** Representative flow cytometry and
22 scatter plots of NCR1+ cell proportions and median fluorescent intensity (MFI) within CD122+

population. (HFD: n=18, LFD: n=14). Data represented as mean ± SD for panels C-E; *P*-values from unpaired Student's t-tests.

FIGURE 3. Exposure to a HFD promotes uNK activation. A) DBA+ cell diameter measurements (µm) and photomicrographs of DBA (DBA: red, DAPI/nuclei: blue) immunofluorescent staining showing the approach for cell diameter measurements (yellow dashed lines). Scale bar = 10µm. (HFD: n=9 implantation sites, LFD: n=9 implantation sites). **B)** Representative flow cytometry plots for analysis of total CD122+CD69+ population and CD69+ population within CD122+NCR1+ cells. **C)** Representative flow cytometry and scatter plots of total CD69+ cell proportions and median fluorescent intensity (MFI) within CD122+ population. (HFD: n=18, LFD: n=14). D) Representative flow cytometry and scatter plots of CD69+ cell proportions and median fluorescent intensity (MFI) within CD122+ NCR1+ population. (HFD: n=18, LFD: n=14). Data represented as mean ± SD; *P*-values from unpaired Student's t-tests for panels A, C, D.

FIGURE 4. HFD leads to impaired spiral artery remodeling. A) Photomicrographs of H&E stained implantation site sections from Gd10.5 displaying the analytical approach used for spiral artery remodeling measurements. **B)** Representative immunofluorescence images Gd7.5 and Gd10.5 implantation sites immunostained with antibodies directed against smooth muscle actin (SMA; purple), and DBA (green); nuclei are stained with DAPI (white). Layers of SMA surrounding the arteries are highlighted with yellow dashed-line, whereas lumens of arteries are depicted in blue-dashed line. Scale bar = 40µm. **C)** Arterial wall area (μm^2) to lumen area (μm^2) [wall:lumen] ratios from Gd10.5. (HFD: n=8 implantation sites, LFD: n=11 implantation sites). **D)** Photomicrographs of H&E stained deciduas from Gd14.5 displaying remodeled uterine arteries. Scale bar = 100µm. Arterial wall area (μm^2) to

lumen area (μm^2) [wall:lumen] ratios from Gd14.5. (HFD: n=18 implantation sites, LFD: n=17 implantation sites). *P*-values from unpaired Student's t-tests for panels C, D.

FIGURE 5. HFD does not affect placental morphology. A) Representative photomicrographs of H&E-stained placentas from HFD- and LFD-fed mice with outlined Labyrinth (L), Junctional zone (Jz) and decidua (D) and scatter plots showing total placental areas (mm^2) from both groups. Scale bar = 1000µm. Scatter plots showing measurements of **B)** labyrinth, **C)** junctional zone and **D)** decidual area ratios to total placental area. HFD: n=24 implantation sites, LFD: n=28 implantation sites; data represented as mean ± SD; *P*-values from unpaired Student's t-tests for panels B-D.

FIGURE 6. HFD modestly affects uNK cytokine expression. Scatter plots showing relative mRNA levels of **A)** TNFα, **B)** MMP-2, **C)** IFNγ and **D)** VEGFA in uNK isolated at Gd10.5. HFD: n=5, LFD: n=5; data represented as mean ± SD; *P*-values from unpaired Student's t-tests for panels A-D.

Figure 1.

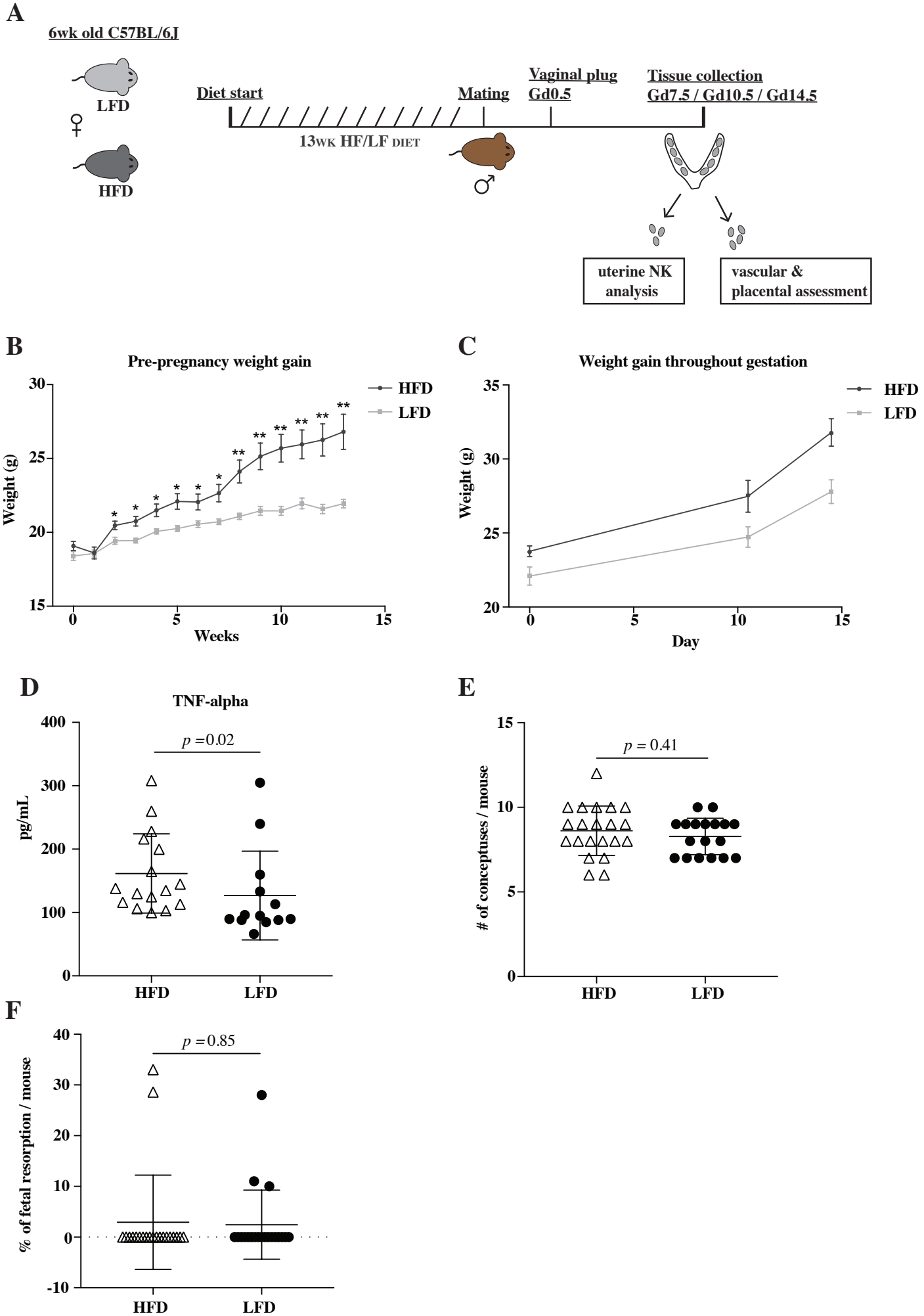
A
6wk old C57BL/6J
LFD
HFD
Diet start
13wk HF/LF diet
Mating
Vaginal plug
Gd0.5
Tissue collection
Gd7.5 / Gd10.5 / Gd14.5
uterine NK analysis
vascular & placental assessment
B
Pre-pregnancy weight gain
Weight (g)
Weeks
HFD
LFD
C
Weight gain throughout gestation
Weight (g)
Day
HFD
LFD
D
TNF-alpha
pg/mL
p =0.02
HFD
LFD
E
# of conceptuses / mouse
p = 0.41
HFD
LFD
F
% of fetal resorption / mouse
p =0.85
HFD
LFD

Figure 2.

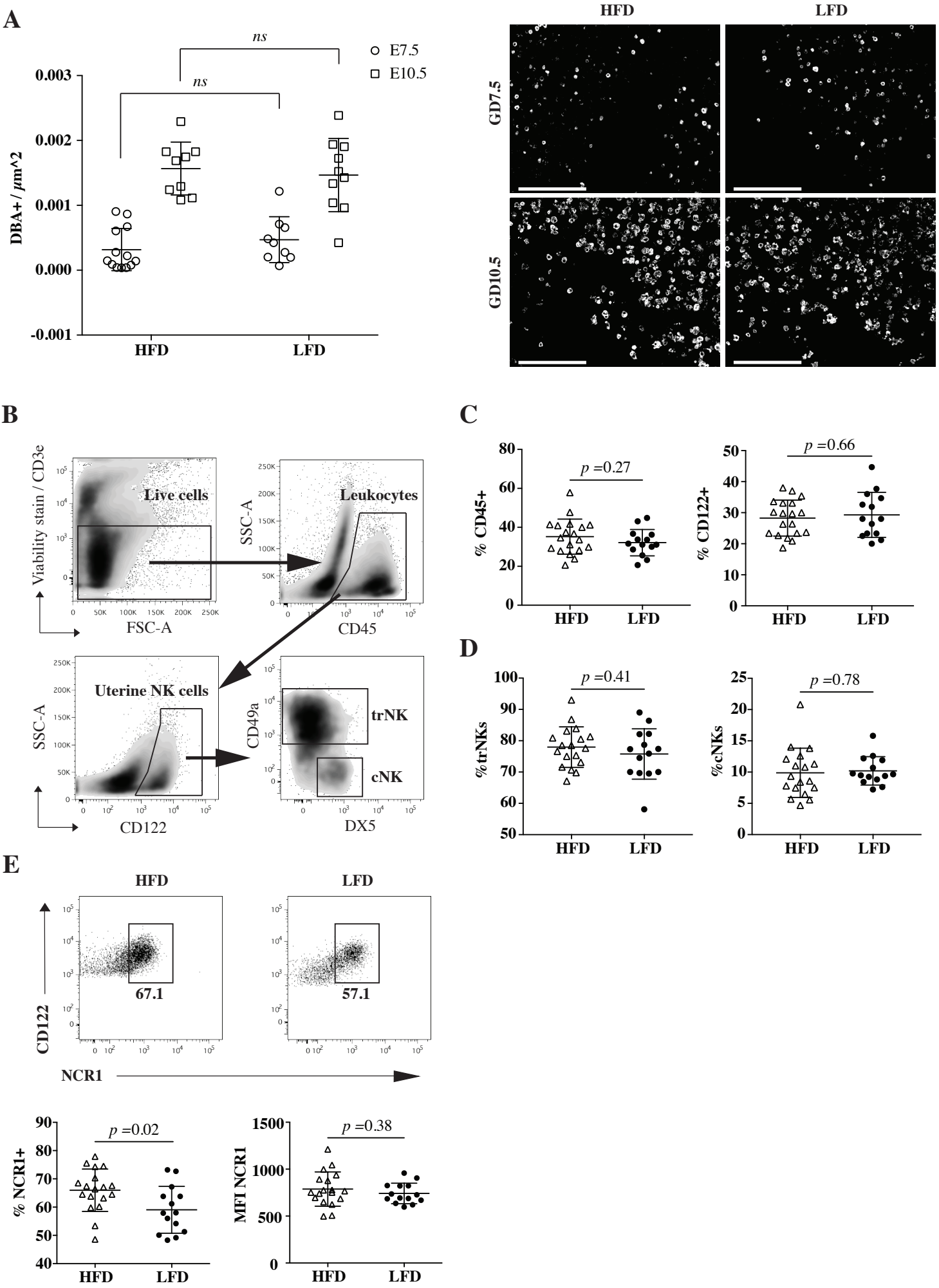
A
ns
ns
E7.5
E10.5
DBA+ / μm^2
0.003
0.002
0.001
0.000
-0.001
HFD
LFD
HFD
LFD
GD7.5
GD10.5
B
Viability stain / CD3e
Live cells
FSC-A
SSC-A
Leukocytes
CD45
SSC-A
Uterine NK cells
CD122
CD49a
trNK
cNK
DX5
C
% CD45+
p =0.27
% CD122+
p =0.66
HFD
LFD
D
%trNKs
p =0.41
%cNKs
p =0.78
HFD
LFD
E
HFD
LFD
67.1
57.1
CD122
NCR1
% NCR1+
p =0.02
MFI NCR1
p =0.38
HFD
LFD

Figure 3.

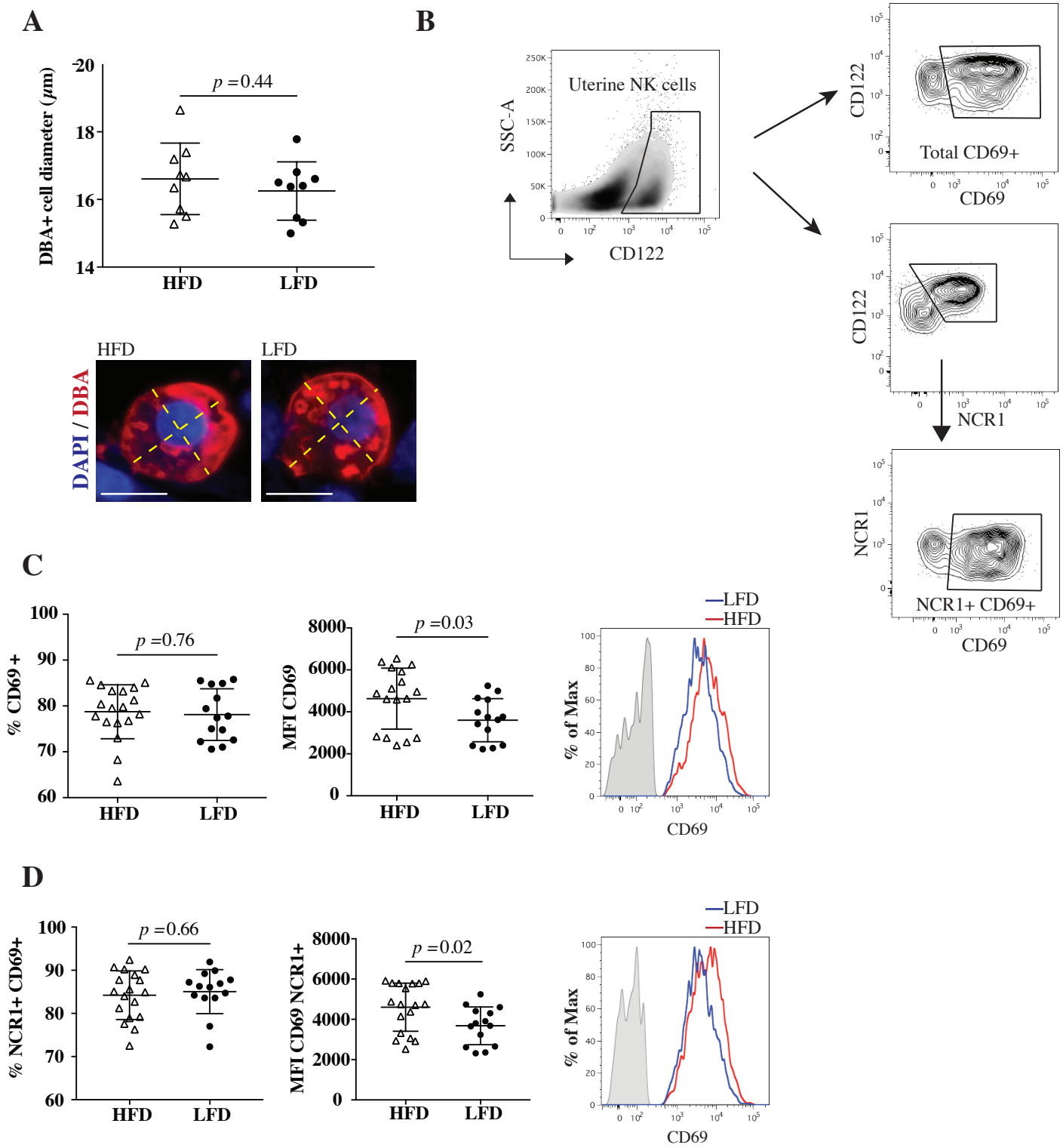
A
DBA+ cell diameter (μm)
p =0.44
HFD
LFD
HFD
LFD
DAPI / DBA
B
Uterine NK cells
SSC-A
CD122
CD122
Total CD69+
CD69
CD122
NCR1
NCR1
NCR1+ CD69+
CD69
C
% CD69+
p =0.76
HFD
LFD
MFI CD69
p =0.03
HFD
LFD
LFD
HFD
% of Max
CD69
D
% NCR1+ CD69+
p =0.66
HFD
LFD
MFI CD69 NCR1+
p =0.02
HFD
LFD
LFD
HFD
% of Max
CD69

Figure 4.

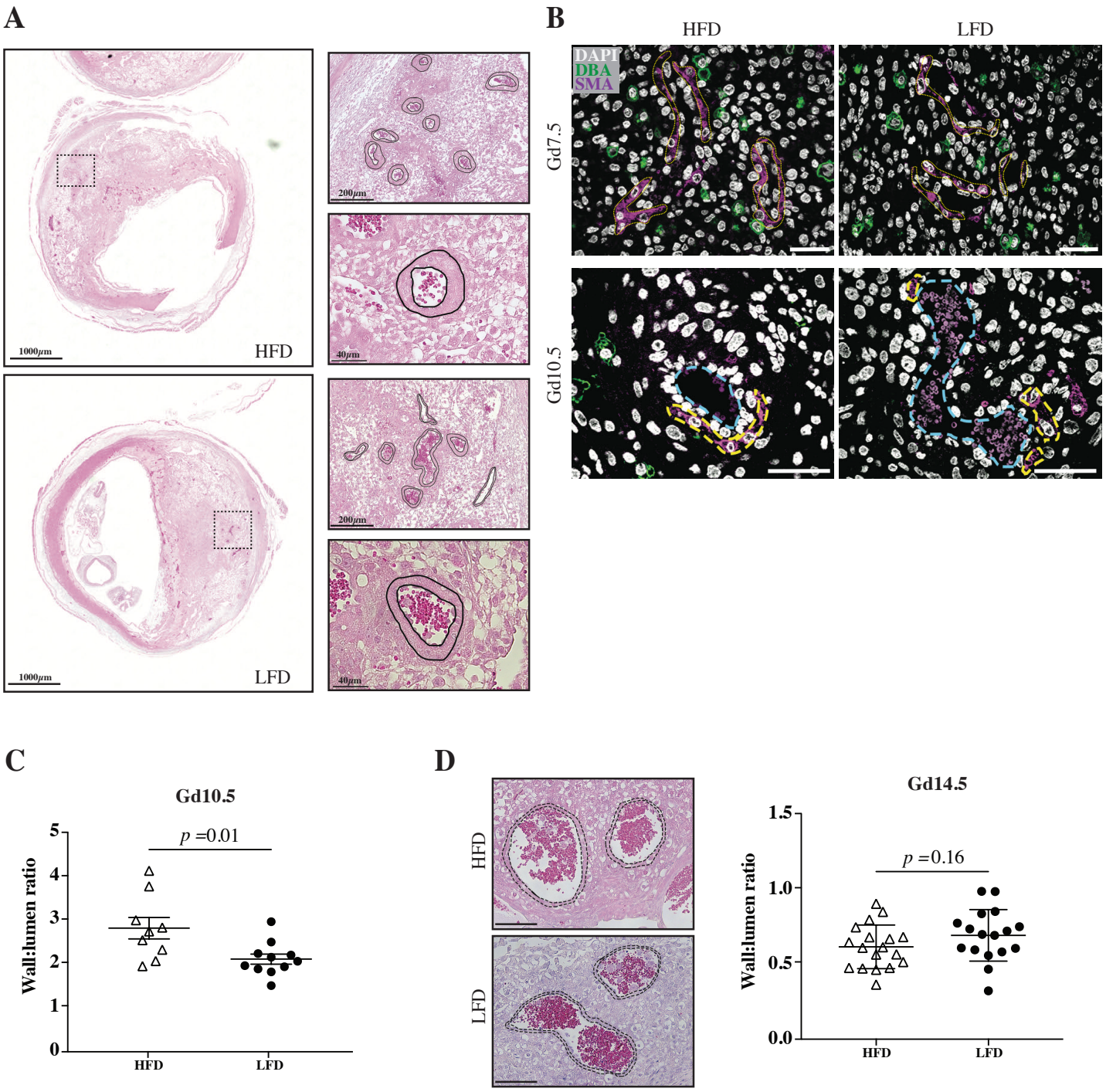
A
1000μm
HFD
200μm
40μm
1000μm
LFD
200μm
40μm
B
HFD
LFD
DAPI
DBA
SMA
Gd7.5
Gd10.5
C
Gd10.5
p =0.01
Wall:lumen ratio
5
4
3
2
1
0
HFD
LFD
D
HFD
LFD
Gd14.5
p =0.16
Wall:lumen ratio
1.5
1.0
0.5
0.0
HFD
LFD

Figure 5.

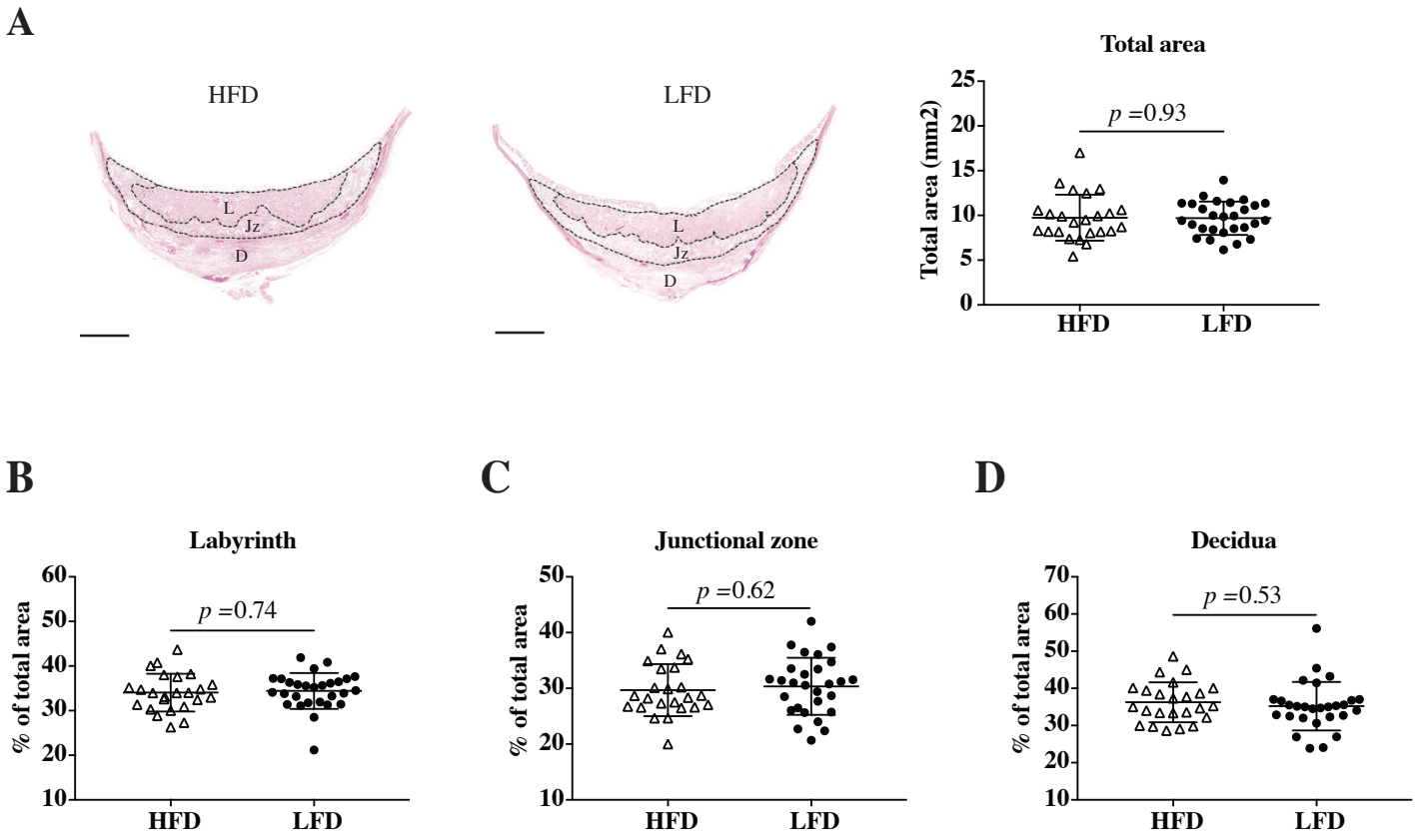
A
HFD
LFD
L
Jz
D
Total area
Total area (mm2)
p =0.93
HFD
LFD
B
Labyrinth
% of total area
p =0.74
C
Junctional zone
p =0.62
D
Decidua
p =0.53

Figure 6.

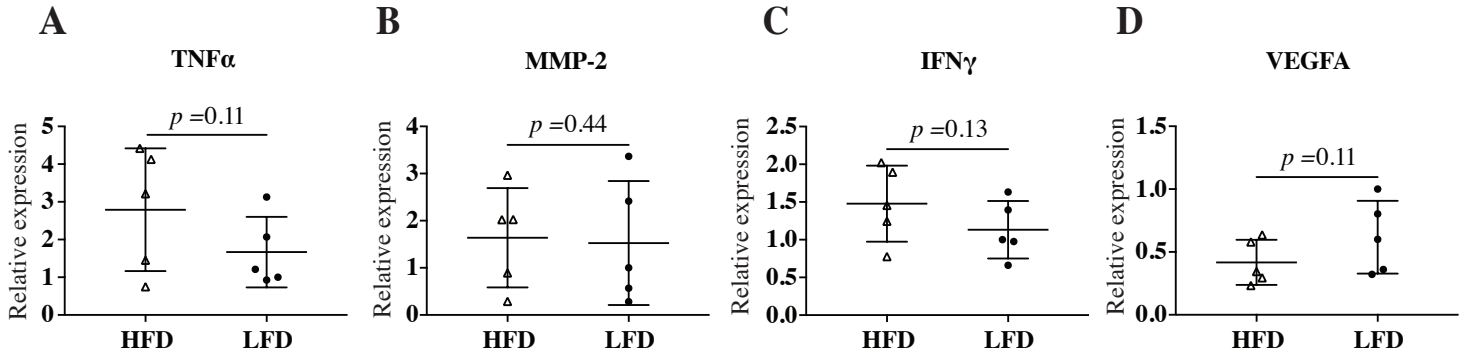
A
TNFα
p =0.11
Relative expression
5
4
3
2
1
0
HFD
LFD
B
MMP-2
p =0.44
Relative expression
4
3
2
1
0
HFD
LFD
C
IFNγ
p =0.13
Relative expression
2.5
2.0
1.5
1.0
0.5
0.0
HFD
LFD
D
VEGFA
p =0.11
Relative expression
1.5
1.0
0.5
0.0
HFD
LFD